This is an open access article published under an ACS AuthorChoice License, which permits copying and redistribution of the article or any adaptations for non-commercial purposes.

Environmental Science & Technology

pubs.acs.org/est

Article

Global Estimates and Long-Term Trends of Fine Particulate Matter Concentrations (1998−2018)

Melanie S. Hammer,* Aaron van Donkelaar, Chi Li, Alexei Lyapustin, Andrew M. Sayer, N. Christina Hsu, Robert C. Levy, Michael J. Garay, Olga V. Kalashnikova, Ralph A. Kahn, Michael Brauer, Joshua S. Apte, Daven K. Henze, Li Zhang, Qiang Zhang, Bonne Ford, Jeffrey R. Pierce, and Randall V. Martin

Cite This: *Environ. Sci. Technol.* 2020, 54, 7879−7890

Read Online

ACCESS | Metrics & More | Article Recommendations | Supporting Information

ABSTRACT: Exposure to outdoor fine particulate matter ($PM_{2.5}$) is a leading risk factor for mortality. We develop global estimates of annual $PM_{2.5}$ concentrations and trends for 1998−2018 using advances in satellite observations, chemical transport modeling, and ground-based monitoring. Aerosol optical depths (AODs) from advanced satellite products including finer resolution, increased global coverage, and improved long-term stability are combined and related to surface $PM_{2.5}$ concentrations using geophysical relationships between surface $PM_{2.5}$ and AOD simulated by the GEOS-Chem chemical transport model with updated algorithms. The resultant annual mean geophysical $PM_{2.5}$ estimates are highly consistent with globally distributed ground monitors (R^2 = 0.81; slope = 0.90). Geographically weighted regression is applied to the geophysical $PM_{2.5}$ estimates to predict and account for the residual bias with $PM_{2.5}$ monitors, yielding even higher cross validated agreement (R^2 = 0.90−0.92; slope = 0.90−0.97) with ground monitors and improved agreement compared to all earlier global estimates. The consistent long-term satellite AOD and simulation enable trend assessment over a 21 year period, identifying significant trends for eastern North America (−0.28 ± 0.03 $\mu g/m^3/yr$), Europe (−0.15 ± 0.03 $\mu g/m^3/yr$), India (1.13 ± 0.15 $\mu g/m^3/yr$), and globally (0.04 ± 0.02 $\mu g/m^3/yr$). The positive trend (2.44 ± 0.44 $\mu g/m^3/yr$) for India over 2005−2013 and the negative trend (−3.37 ± 0.38 $\mu g/m^3/yr$) for China over 2011−2018 are remarkable, with implications for the health of billions of people.

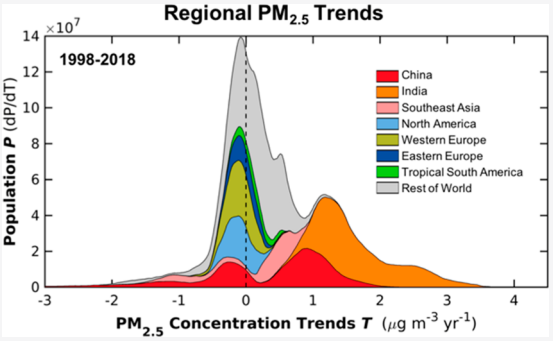

INTRODUCTION

Exposure to ambient fine particulate matter ($PM_{2.5}$) is the leading environmental risk factor for the global burden of disease[1] with an estimated 3 million attributable deaths worldwide in 2017. Additionally, the World Health Organization (WHO) estimates that 92% of the world's population lives in areas with annual mean $PM_{2.5}$ greater than 10 $\mu g/m^3$, exceeding their air quality guideline for $PM_{2.5}$ exposure.[2] International assessments require global estimates of $PM_{2.5}$.[1−4] However, large gaps exist in ground-based monitoring of $PM_{2.5}$.[5] Satellites and global models are critical for constraining the magnitude and trends in concentrations of $PM_{2.5}$ globally and for quantifying exposure-health relationships.[6] Recent developments in satellite products, chemical transport model simulations, and ground monitor sampling offer exciting opportunities to improve global $PM_{2.5}$ estimates and to evaluate ambient $PM_{2.5}$ concentrations and trends for the past 20+ years.

Several recent advancements in satellite-retrieved aerosol optical depth (AOD) offer the prospect of improving global $PM_{2.5}$ estimates. Collection 6.1 (C6.1) of MODIS (MODerate resolution Imaging Spectroradiometer) retrieved AOD includes updated radiometric calibration improving the stability of MODIS measured radiances over the entire record and important updates to the Dark Target (DT)[7] and Deep Blue (DB)[8,9] algorithms. The MAIAC (Multi-Angle Implementation of Atmospheric Correction) algorithm[10] provides AOD retrieved from MODIS C6 radiances at a resolution of 1 km and is now extended to global coverage for the entire MODIS record. The recently released MISR (Multiangle Imaging Spectroradiometer) version 23 algorithm[11,12] now provides AOD retrievals at 4.4 km resolution, finer than the 17.6 km resolution of the previous version 22.

Received: March 20, 2020
Revised: June 1, 2020
Accepted: June 3, 2020
Published: June 3, 2020

Downloaded via NOAA CENTRAL LIBRARY on September 13, 2021 at 17:11:38 (UTC).
See https://pubs.acs.org/sharingguidelines for options on how to legitimately share published articles.

Concurrent development of chemical transport models offers an improved characterization of the $PM_{2.5}$ distribution and the geophysical relationship of AOD to $PM_{2.5}$. A recent assimilation (MERRA-2)[13] provides consistent meteorological inputs for 1979−present. Improved representations of secondary organic aerosol[14,15] and fine dust[16,17] better simulate surface $PM_{2.5}$ concentrations. The development of an anthropogenic fugitive, combustion, and industrial dust (AFCID) emission inventory now represents anthropogenic crustal material.[18] An updated fire emissions inventory (GFED4)[19] provides increased global coverage and finer resolution biomass burning emissions. Significant updates to regional anthropogenic emissions inventories of aerosols and their precursors over China,[20] elsewhere in Asia,[20] the United States,[21] and Europe (http://www.emep.int) provide improved time-varying information, especially for recent years.

The ground-based $PM_{2.5}$ measurement network has expanded considerably in recent years with 3787 direct $PM_{2.5}$ monitor sites in 2015,[22] increasing monitor density particularly in China and India. Improved statistical methods have been developed to obtain estimates of surface $PM_{2.5}$ concentrations from satellite AOD and ground monitor data, including empirical relationships between satellite AOD and $PM_{2.5}$ from ground monitors,[23,24] Land Use Regression (LUR) models in conjunction with satellite AOD,[25] and Geographically Weighted Regression (GWR) with meteorological and land use information with satellite AOD at $PM_{2.5}$ monitor sites.[26,27] Several studies have found that including geophysical fields from a chemical transport model aids statistical fusion at large spatial scales.[28−32]

In this work, we leverage recent developments in satellite AOD, chemical transport modeling, and ground monitor data to produce global satellite-derived $PM_{2.5}$ estimates with long-term consistency for trend assessment over 21 years, for 1998−2018. As risk estimates for chronic exposure per increment of $PM_{2.5}$ are approximately an order of magnitude larger than for acute exposures,[33,34] we therefore focus on the annual scale to be most applicable to health impact studies, as these are the basis for most assessments and given that most concentration response functions that connect $PM_{2.5}$ to health outcomes were developed using annual-average concentrations.[1,2,35−37] In addition, ground monitor data used for comparison is most consistently available globally on an annual mean basis. We combine satellite AOD from SeaWiFS (Sea-Viewing Wide Field-of-View Sensor) and the newly released MAIAC, MISRv23, and C6.1 MODIS products. We conduct an updated simulation using the global chemical transport model GEOS-Chem to represent the geophysical relationship between $PM_{2.5}$ and AOD and as an additional AOD source. We investigate the impact of these changes on previous satellite-derived $PM_{2.5}$ estimates that follow a similar methodology.[29] Taking advantage of the improved long-term consistency in satellite AOD and simulated meteorology, we calculate the 21-year trends in the satellite-derived $PM_{2.5}$ values and examine the monthly population-weighted mean time series. We then statistically fuse the $PM_{2.5}$ surface with an updated version of the recently released ground monitor data set from the World Health Organization (WHO) and investigate the impact of increased ground-based monitoring. We examine the regional distributions of population as a function of (1) $PM_{2.5}$ concentrations and (2) 1998−2018 $PM_{2.5}$ trends to gain insight into the distribution of ambient $PM_{2.5}$ effects worldwide.

METHODS

Satellite AOD Sources. A detailed description of the satellite AOD sources used is given in the Supporting Information S1. We use AOD retrieved from radiances measured by four satellite instruments: twin MODIS instruments, the MISR instrument, and the SeaWiFS instrument.

The twin MODIS instruments have flown on the Terra and Aqua satellites since 2000 and 2002, respectively, providing daily global coverage.[38] We use AOD retrieved from three retrieval algorithms that process MODIS measured radiances: Dark Target (DT), Deep Blue (DB), and MAIAC.

The DT retrieval algorithm[39] is designed to retrieve AOD over dark surfaces (e.g., vegetated land surfaces and dark soils). The DB retrieval algorithm[9] uses blue wavelength measurements where the surface reflectance over land is typically much lower than at longer wavelengths, allowing for the retrieval of aerosol properties over both bright and dark surfaces. We use the recently released collection 6.1 of the MODIS retrieved AOD products, which include spatial resolution of 10 km and several updates to the DT[7] and DB[8,9]algorithms.

The MAIAC algorithm[10] retrieves AOD at a spatial resolution of 1 km over both bright and dark land surfaces. MAIAC was officially released in May 2018, providing AOD globally for the entire MODIS record. However, this work started earlier and used an internally released MAIAC data set consistent with the global release but lacking parts of Canada, eastern Siberia, and the Indo-Pacific region.

The SeaWiFS instrument flew on the SeaStar satellite and was operational between 1997 and 2010. SeaWiFS maintained a highly accurate and stable calibration over its lifetime,[40] providing daily global coverage. We use the version 4 SeaWiFS Deep Blue[40,41] data set with a spatial resolution of 13.5 km.

The MISR instrument is onboard the Terra satellite along with MODIS and has been operational since 2000 providing global coverage once per week.[42] The MISR retrieval algorithm provides AOD retrievals over bright and dark land surfaces.[43] We use AOD retrieved from the recently released MISRv23 algorithm,[11,44] which provides AOD at a spatial resolution of 4.4 km, a significant improvement over the 17.6 km resolution in the previous version of MISRv22.

Simulated Relationship of Surface $PM_{2.5}$ and Total Column AOD. To estimate surface concentrations of $PM_{2.5}$ from satellite AOD (AOD_{SAT}), we use the local, coincident ratio (η) of simulated surface $PM_{2.5}$ concentrations ($PM_{2.5,SIM}$) to simulated total column AOD (AOD_{SIM}):

$$PM_{2.5,SAT} = \eta \times AOD_{SAT} \quad (1)$$

where

$$\eta = PM_{2.5,SIM}/AOD_{SIM} \quad (2)$$

η is a function of the factors that relate $PM_{2.5}$ mass to satellite observations of AOD (e.g., aerosol size, aerosol composition, diurnal variation, relative humidity, and the vertical structure of aerosol extinction[45]). A full derivation of η is found in the work of van Donkelaar et al.[46] To account for differences in temporal sampling of the AOD data sources, we calculate daily values of η as the ratio of 24-h ground-level $PM_{2.5}$ at a relative humidity of 35%, to total-column AOD at ambient relative humidity sampled at satellite overpass time.

The ability to calculate accurate η values depends on the simulation's ability to accurately model the relationship between $PM_{2.5}$ concentrations and AOD. We use v11−01 of

https://dx.doi.org/10.1021/acs.est.0c01764
Environ. Sci. Technol. 2020, 54, 7879−7890

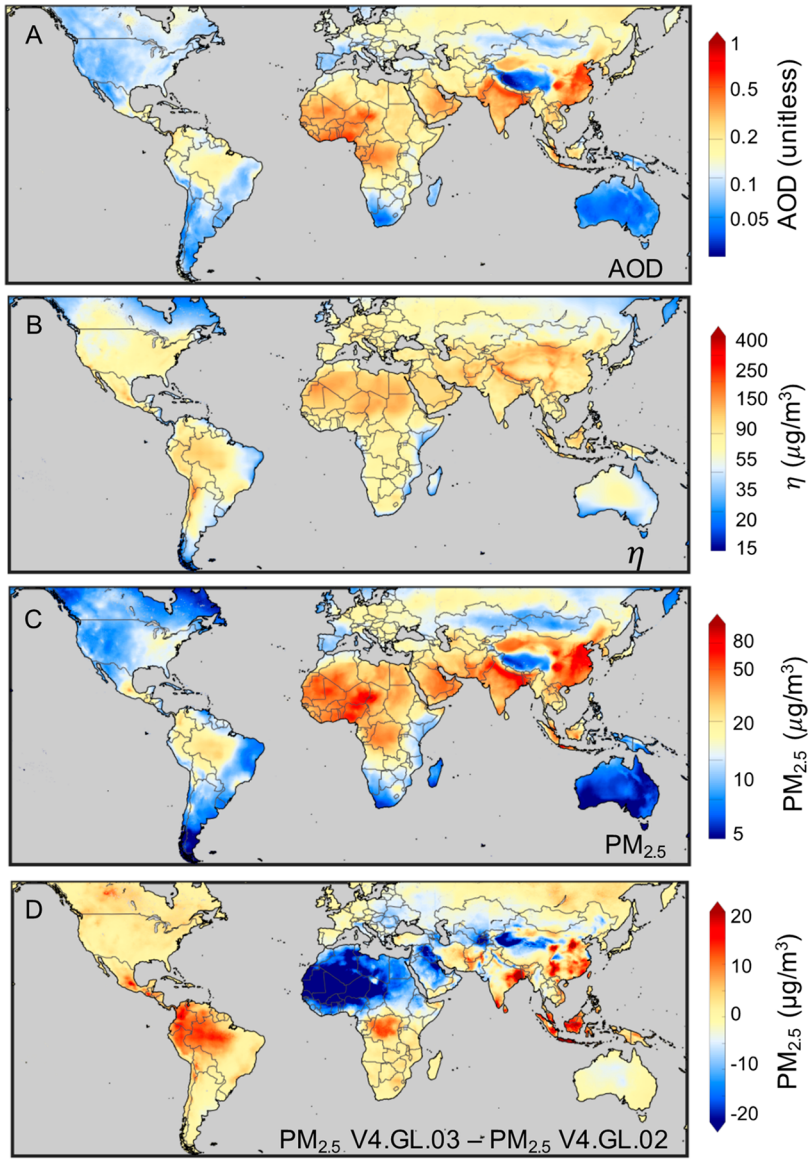

Figure 1. Combined AOD (A), simulated η ($PM_{2.5}$/AOD) (B), and combined $PM_{2.5}$ estimates (C) for 1998−2018. The logarithmic $PM_{2.5}$ color scale (C) is directly proportional to the logarithmic AOD (A) and η (B) color scales, obtained by normalizing the global average AOD and global average η to that of $PM_{2.5}$. The bottom panel (D) shows the difference between this updated version (V4.GL.03) of geophysical $PM_{2.5}$ estimates and the previous version (V4.GL.02) from van Donkelaar et al.[29] for 2011−2016. Gray denotes water.

the GEOS-Chem chemical transport model (http://geos-chem.org). A detailed description of the simulation is included in the Supporting Information (SI). Our simulation is driven by assimilated meteorological data from the recent MERRA-2 Reanalysis of the NASA Global Modeling and Assimilation Office (GMAO), which offers a consistent assimilation from 1979.[47] We conduct our simulation for the years 1998−2018 with 47 vertical layers at a spatial resolution of 2° × 2.5° with a nested resolution of 0.5° × 0.625° over North America, Europe, and China. The top of lowest model layer is ∼100 m. Our simulation includes improved representations of secondary organic aerosol[14,15] and fine dust[16,17] which better simulate surface PM concentrations. We use the AFCID emission inventory, which now provides a representation of anthropogenic crustal material.[18] An updated version of GFED4 provides increased global coverage and finer resolution biomass burning emissions[19] over the entire period of interest (1998−2018). We include updated regional anthropogenic emission inventories (summarized in SI Table S2) of aerosols and their precursors over China (MEIC[20]), India (Lu et al.[48]), elsewhere in Asia (MIX[20]), the United States (EPA/NEI11[21]), and Europe (EMEP; http://www.emep.int).

Combined $PM_{2.5}$ Estimated from Satellites and Simulation. We calculate geophysical $PM_{2.5}$ estimates following the work of van Donkelaar et al.,[29] with updates to (1) ground-based $PM_{2.5}$ and AOD measurements, (2) satellite AOD products, (3) GEOS-Chem simulation, and (4) resolution of our analysis. A detailed description of the algorithm is provided in van Donkelaar et al.[29] and in the Supporting Information. A summary of the satellite AOD sources can be found in Table S1a, while a summary of the other data sources used can be found in Table S1b. There are two main steps of the algorithm: the intercalibration of the satellite and simulated AOD sources and the calculation of combined $PM_{2.5}$ from the calibrated AOD sources.

https://dx.doi.org/10.1021/acs.est.0c01764
Environ. Sci. Technol. 2020, 54, 7879−7890

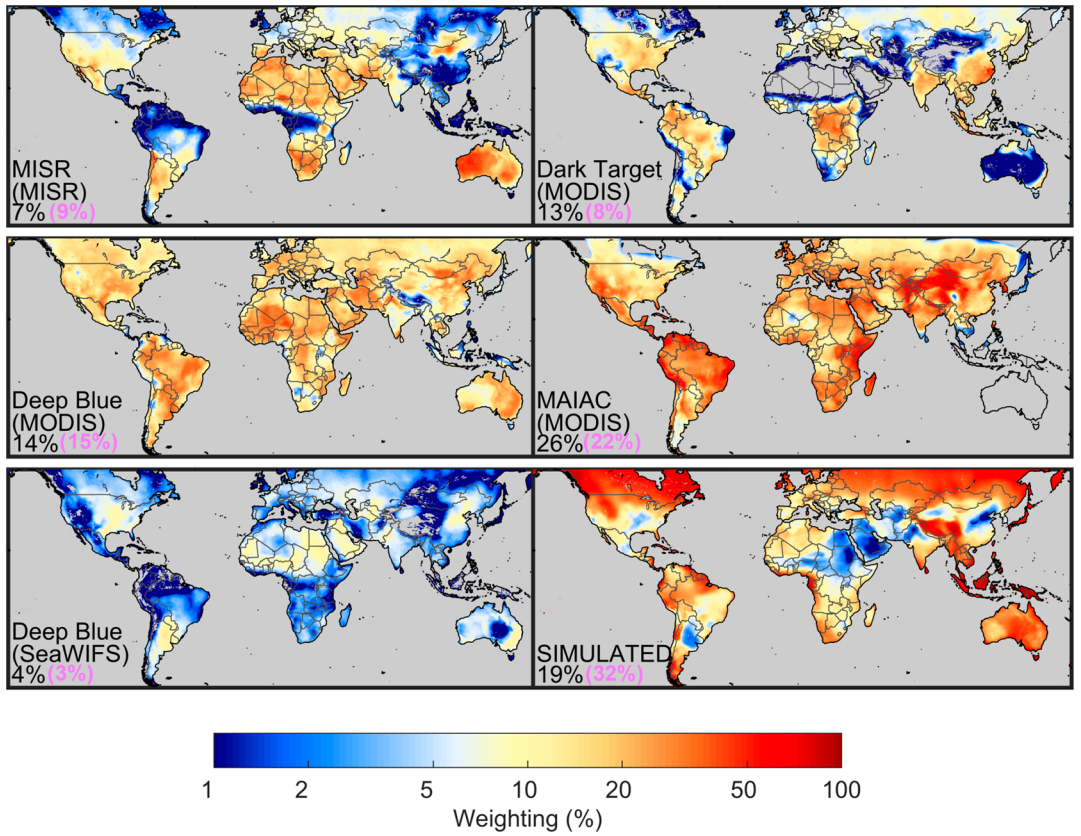

Figure 2. Mean contribution of each source to the combined $PM_{2.5}$ estimate for 2000−2018. Values in black in the bottom left of each panel indicate the population-based mean weighting at locations with available data, while purple values indicate the area-based mean weighting. The retrieval algorithm name is given in the lower left of each panel, with the instrument name in parentheses. Dark Target and Deep Blue MODIS correspond to Terra-based retrievals only. Gray denotes missing data or water.

For the intercalibration of satellite and simulated AOD sources, each source is first translated onto a common 0.05° × 0.05° grid by area-weighting satellite retrievals and linearly interpolating simulated values. This resolution is finer than the 0.1° × 0.1° resolution used previously,[29] given the finer resolution provided by the new versions of MISR (4.4 km) and MAIAC (1 km) AOD. For a consistent definition of uncertainty, we compare the daily satellite AOD values from each data set with daily AOD measurements at 550 nm from AERONET (Aerosol Robotic Network),[49] a global sun photometer network that provides AOD measurements with high accuracy (uncertainty <0.02).[50] We use level 2 of the recently released version 3 AERONET data.[51]

The different sources of error associated with satellite and simulated AOD require care in accounting for their relative uncertainties.[29] Briefly, one of the main sources of uncertainty associated with satellite retrieved AOD is the surface treatment used in the retrieval,[52] which we assess by comparison with AERONET as a function of land type. For the simulated AOD, to account for errors due to species-specific emissions and assumed aerosol microphysical properties, we calculate the relative uncertainty based on the simulated fractional aerosol composition applied to each daily AERONET observation following van Donkelaar et al.[53] Figure S1 shows a scatterplot of our combined monthly AOD estimates versus AERONET AOD for 2015, illustrating a high degree of consistency (R^2 = 0.84; slope = 0.97).

The daily surface $PM_{2.5}$ concentrations from each data source are obtained by applying the daily simulated AOD to $PM_{2.5}$ ratios (η) to the coincident daily calibrated AOD sources. Monthly means are calculated from the daily $PM_{2.5}$ values. The monthly mean $PM_{2.5}$ concentrations from each source are then combined using a weighted average (eq S4). Where available, spatial information from the 1 km MAIAC AOD retrieval is incorporated by applying the monthly climatology of its retrieved relative variation between 0.01° and 0.05°. Where MAIAC is unavailable, monthly AOD and $PM_{2.5}$ are linearly interpolated onto a 0.01° × 0.01° grid. The monthly mean $PM_{2.5}$ concentrations are then aggregated to annual mean values.

Hybrid $PM_{2.5}$ Estimates. We use geographically weighted regression (GWR)[54,55] to predict and account for the bias in the annual mean of our geophysical $PM_{2.5}$ estimates as described by van Donkelaar et al.[29] We perform the GWR between our annual mean geophysical $PM_{2.5}$ estimates and annual $PM_{2.5}$ concentrations measured by ground monitors. We use monitor-specific ground-based measurements of $PM_{2.5}$ from an updated version of the WHO Global Ambient Air Quality Database,[22] which provides annual measurements for the years 2010−2018. Table S3 summarizes the global number of measurements for each year. The predictor variables used in the regression are associated with uncertainties in the simulated relation of $PM_{2.5}$ to AOD, such as simulated aerosol types, subgrid topographical variation, and urban surfaces (eq S5).

https://dx.doi.org/10.1021/acs.est.0c01764
Environ. Sci. Technol. 2020, 54, 7879−7890

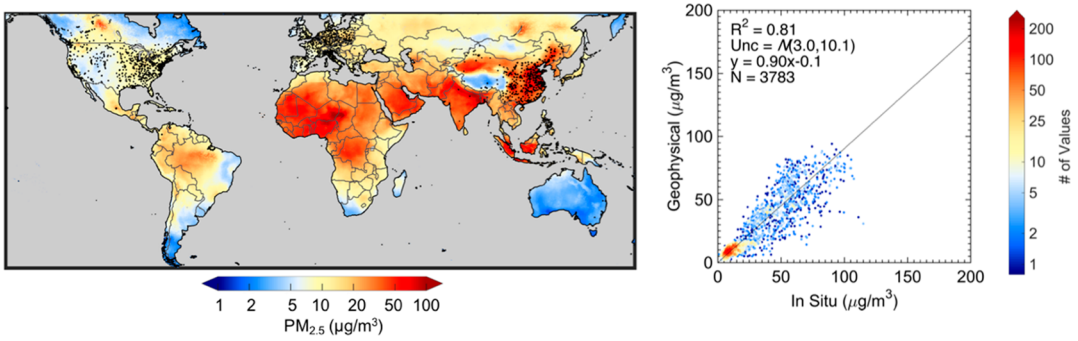

Figure 3. Left: Geophysical $PM_{2.5}$ for 2015. Black dots represent monitor locations. Gray denotes water. Right: Annual mean geophysical $PM_{2.5}$ versus coincident annual mean in situ values for 2015. Included on the plots are the coefficient of variation (R^2), the normal distribution of uncertainty (N(bias, variance)), the line of best fit (y), and the number of comparison points (N). The color scale indicates the number density of observations at each point.

RESULTS AND DISCUSSION

The top three panels of Figure 1 show (A) the combined AOD, (B) simulated η ($PM_{2.5}$/AOD), and (C) combined $PM_{2.5}$ estimates for 1998−2018. The logarithmic $PM_{2.5}$ color scale (C) is directly proportional to the logarithmic AOD (A) and η (B) color scales to facilitate comparison of features between plots. Several factors affect the simulated relation of AOD and $PM_{2.5}$.[45,56] Since AOD is at ambient relative humidity and surface $PM_{2.5}$ is at controlled relative humidity, high η values exist over desert regions in North Africa and the Middle-East partly due to the low hygroscopicity of the aerosols.[45,46] Hygroscopicity decreases η by decreasing dry mass compared with ambient conditions. Higher values over industrial regions in India and eastern China, where aerosols have more water uptake,[57−59] reflect the enhanced near-surface aerosol concentrations in source regions that increase the ground level to columnar fraction. Over southern China, higher AOD compared to surface $PM_{2.5}$ (e.g smaller values) partially reflect the transport of biomass burning aerosol from southeast Asia at high altitudes.[60,61] Relatively low η values over northern regions in Canada and Russia occur where surface $PM_{2.5}$ concentrations are lower and a higher fraction of the aerosol tends to be aloft. Enhanced η values over the Andes and the Tibetan Plateau reflect the diminished AOD column over elevated topography.

The bottom panel of Figure 1D shows the difference between this updated version (V4.GL.03) of geophysical $PM_{2.5}$ estimates and the previous version[29] (V4.GL.02) for 2011−2016. The largest differences are apparent over desert regions, with a decrease in $PM_{2.5}$ concentrations of about −20 $\mu g/m^3$. This difference reflects the influence of the improved dust scheme[16,17] used in the updated GEOS-Chem simulation on simulated η, as the previous version overestimated surface fine dust concentrations.[29] There are increases in $PM_{2.5}$ concentrations of about 5−15 $\mu g/m^3$ over South America, central Africa, India, China, and Southeast Asia, with smaller increases of about 2−5 $\mu g/m^3$ over parts of North America and Russia. These differences reflect the updated anthropogenic[20,21,48] and biomass burning[19] emission inventories and secondary organic aerosol chemistry scheme[14,15] used in the updated GEOS-Chem simulation.

Figure 2 shows the mean area-based weighting over 2000−2018 of each AOD source used in the combined estimate (we chose this time period because prior to 2000 SeaWiFS was the only observing satellite instrument). For MODIS Dark Target and Deep Blue, only Terra-based retrievals are shown, although Aqua is also included in the combined estimate. Therefore, a total of eight sources contribute to the combined product, and an individual source of average quality would have a weighting of approximately 1/8 (12%). Values in black in the bottom-left of each panel indicate the population-based mean weighting at locations with available data, whereas purple values in parentheses indicate the area-based mean weighting. MAIAC contributes the highest percentage to the population-based geophysical $PM_{2.5}$ estimate with a mean weighting of 26% reflecting its strong overall performance including over arid and mountainous regions with difficult surface conditions. The large increase in MAIAC contribution compared to the 12% mean contribution in earlier work[29] is related to its near global coverage, which was not previously available. MODIS Deep Blue performs well over most parts of the world, especially over deserts, with a population-based mean weighting of 14%. MODIS Dark Target (13% population-based) performs well over Central America, central Africa, and Southeast Asia. MISR (7% population-based mean weighting) is strongest over regions with difficult surface conditions such as deserts. SeaWiFS DB is weighted less heavily (4% population-based mean weighting) compared to the other sources, largely due to reduced sampling frequency. Simulated AOD has a population-based mean weighting of 19% from large contributions over northern regions and southeastern Asia where seasonal snow-cover and cloud-cover respectively inhibit satellite retrievals. Overall satellite retrievals comprise most (81%) of the population-weighted AOD contribution due to their accuracy in the majority of regions associated with significant population density.

Figure 3 shows the geophysical $PM_{2.5}$ estimates for 2015. Elevated concentrations are apparent over East Asia and South Asia reflecting a wide variety of sources as extensively discussed in the literature.[60−66] Enhancements over North Africa and the Middle-East are driven by regional mineral dust sources.[67−69] Lower concentrations over North America and western Europe reflect regional emission controls.[70−75] Evaluation of these geophysical estimates versus ground-based measurements yields excellent consistency on an annual mean basis with R^2 = 0.81 and a slope of 0.90. This agreement offers promise for satellite-derived $PM_{2.5}$ in regions with low monitor density, as our geophysical estimates are independent of ground monitor data. Exclusion of GEOS-Chem would reduce the R^2 versus $PM_{2.5}$ monitors to 0.73. Using AOD from only a single satellite retrieval would further reduce the R^2 to 0.50−0.70. Using only AOD from GEOS-Chem would give a R^2 = 0.63. Thus, the

https://dx.doi.org/10.1021/acs.est.0c01764
Environ. Sci. Technol. 2020, 54, 7879−7890

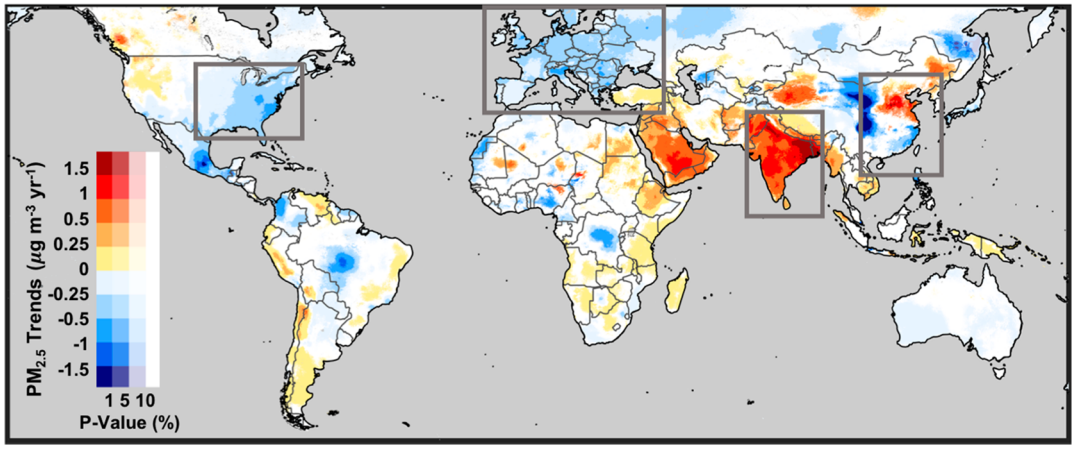

Figure 4. Trends in geophysical $PM_{2.5}$ values calculated from the generalized least-squares regression of monthly time series values during 1998−2018. Warm colors indicate positive trends, cool colors indicate negative trends, and the opacity of the colors indicates the statistical significance of the trends. Gray denotes water. Gray boxes indicate areas featured for regional analysis in Figure 5.

overall consistency with ground measurements is driven by satellite observations complemented by the GEOS-Chem simulation.

The long-term radiometric calibration of the newly released satellite AOD products and the long-term consistency of the meteorology and emissions used in the GEOS-Chem simulation enable assessment of trends. Figure 4 shows the trends in our geophysical $PM_{2.5}$ values for 1998−2018, calculated using generalized least-squares regression (GLS)[76,77] as implemented by Boys et al.[78] There are statistically significant (p-value <0.05) positive trends in $PM_{2.5}$ exceeding 1 $\mu g/m^3/yr$ throughout India and of 0.25 to 0.5 $\mu g/m^3/yr$ across the Middle East, central and southern Africa, and Canada. There is a small area of positive trends (~1 $\mu g/m^3/yr$) over eastern China and a small region of negative trends (−1 $\mu g/m^3/yr$) over northern China; however, most of East Asia does not exhibit statistically significant trends when taken over the entire time period. There are statistically significant, negative trends in $PM_{2.5}$ values (−1 to −0.25 $\mu g/m^3/yr$) over the eastern US, Europe, central South America, and Australia.

Figure 5 shows the regional time-series calculated using the GLS of monthly population-weighted mean (PWM) geophysical $PM_{2.5}$ anomalies for the eastern US, Europe, East Asia, and India. The time-series plots for the eastern US and Europe exhibit negative trends, with slopes of −0.28 ± 0.03 $\mu g/m^3/yr$ and −0.15 ± 0.03 $\mu g/m^3/yr$, respectively. These negative trends reflect the emission controls implemented in these regions.[70−75] There is a positive trend in PWM $PM_{2.5}$ concentrations over India with a slope of 1.13 ± 0.15 $\mu g/m^3/yr$, reflecting the increasing emissions of anthropogenic aerosol and their precursors.[48,79] However, a single linear trend in India and East Asia is potentially misleading due to abrupt changes in the trends throughout the 1998−2018 period. Three separate regimes are visible over India: a positive trend (slope 0.93 ± 0.39 $\mu g/m^3/yr$; pink) for 1998−2007, a period of a large positive trend (slope 2.44 ± 0.44 $\mu g/m^3/yr$; green) for ~2005−2013 which drives the positive 1998−2018 trend, then a negative trend (slope −0.55 ± 0.70 $\mu g/m^3/yr$; dark purple) for 2011−2018. Over East Asia, a positive trend in PWM $PM_{2.5}$ concentrations (slope 0.93 ± 0.19 $\mu g/m^3/yr$; yellow) is visible until about 2012, after which the trend becomes strongly negative (slope −3.67 ± 0.38 $\mu g/m^3/yr$; fuschia). This recent negative trend is the most rapid regional decrease in $PM_{2.5}$ concentrations apparent worldwide since the year 1998, reflecting the emission controls placed on SO_2 and NO_x in China after 2012.[48,80−82] Overall, global PWM $PM_{2.5}$ increased by 0.04 ± 0.02 $\mu g/m^3/yr$ (Table S5).

The regional timeseries for the eastern U.S., Europe, and China are coincidently sampled and evaluated against ground measurements in Figure S2. Over the eastern US (top panel) evaluation of the timeseries of coincidently sampled EPA ground measurements for 1999−2016 indicates excellent consistency (slope −0.44 ± 0.05 $\mu g/m^3/yr$ geophysical $PM_{2.5}$; −0.43 ± 0.03 $\mu g/m^3/yr$ ground measurements). Evaluation of trends over Europe and China is impeded by the shorter time periods with available ground-based measurements, but the linear tendencies nonetheless are consistent within their uncertainties. Over India, the lack of available long-term measurements prohibited evaluation there.

We next statistically fuse the geophysical estimates of $PM_{2.5}$ with in situ ground monitor data. Figure S3 shows the predicted bias from GWR, while Figure S4 shows the net impact of the individual predictors on the predicted bias. Figure 6 shows the resulting statistically fused (hybrid) estimates for 2015. The scatterplot shows 10-fold out-of-sample 10% cross validation at sites that were not used in the GWR regression. Statistical fusion explains 11% of the variance in the ground-based measurements, increasing to R^2 = 0.92. The agreement for the entire data set of hybrid $PM_{2.5}$ values was very similar (R^2 = 0.90) to the agreement of just the cross-validated sites described above, suggesting the impact of overfitting is small, and is comparable to other recent statistical fusion techniques.[30]

The agreement of our hybrid $PM_{2.5}$ estimates (V4.GL.03) with ground monitors is significantly improved compared to the agreement of V4.GL.02 in van Donkelaar et al.[29] for more recent years (2014−2016), as shown in SI Table S4. The weak change in the agreement among years 2014−2016, when there was still a significant increase in the number of monitors, suggests that estimates would benefit from increasing monitor density in underrepresented regions (e.g., India, Africa, the Middle-East, and South America), rather than increasing the number of monitors in regions where they are already available (i.e., North America, Europe, and China).

https://dx.doi.org/10.1021/acs.est.0c01764
Environ. Sci. Technol. 2020, 54, 7879−7890

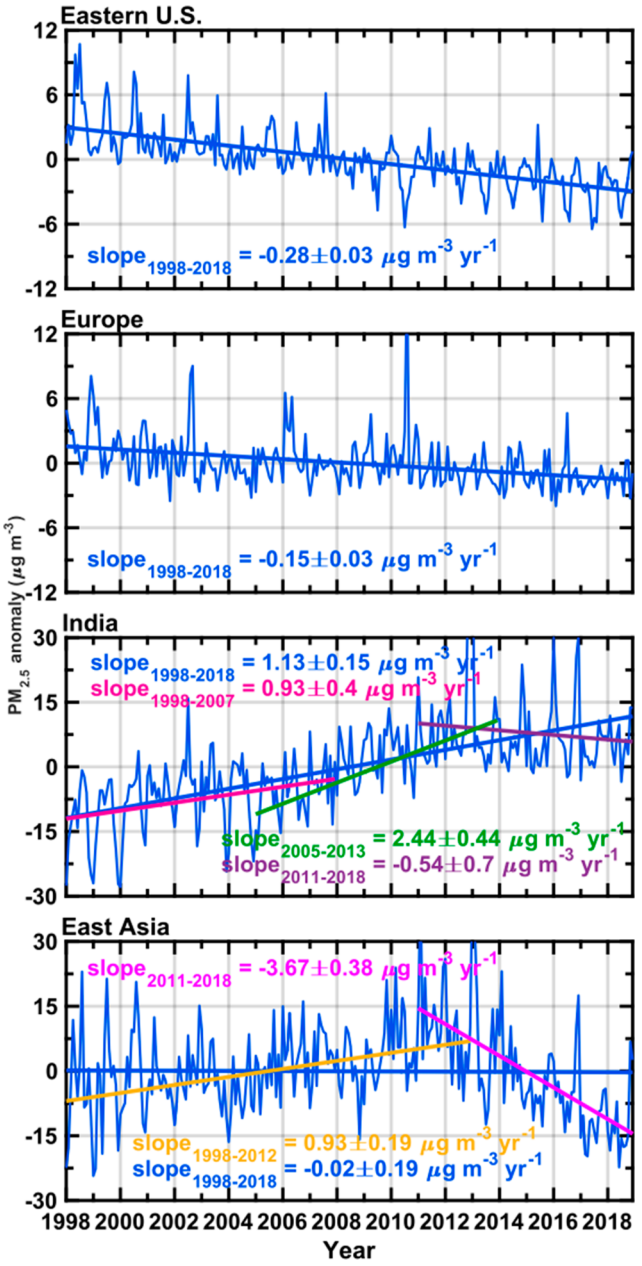

Figure 5. Regional monthly time series anomaly plots of population-weighted mean geophysical $PM_{2.5}$ values for 1998−2018 with their corresponding linear fits (with the slope ± standard error) in blue. In the third panel, the 1998−2007 linear fit over India is shown in pink, the 2005−2013 linear fit is shown in green, and the 2011−2018 linear fit is shown in purple. In the bottom panel, the 1998−2012 linear fit over East Asia is shown in yellow, while the 2011−2018 linear fit is shown in magenta. Population estimates are from the Gridded Population of the World (GPW v4) database,[87] and unavailable years were obtained via linear interpolation.

Table S5 shows the regional population-weighted mean $PM_{2.5}$ for our estimates compared to the 2017 Global Burden of Disease data set. Our hybrid $PM_{2.5}$ estimates (V4.GL.03) at monitor locations (PWM 43.2 $\mu g/m^3$) are more consistent with $PM_{2.5}$ measurements (PWM 44.9 $\mu g/m^3$) than are recent estimates from the Global Burden of Disease[30] (PWM 50.8 $\mu g/m^3$). The regional root-mean-square error (RMSE) values for our GWR-adjusted hybrid estimates compared to the out-of-sample values are shown in Table S6. Our out-of-sample population-weighted RMSE of 6.8 $\mu g/m^3$ is lower than all prior estimates to date (e.g., Shaddick et al.[30]). These tables also demonstrate the need for increased ground monitoring in regions such as South America and Africa where scarce measurement data inhibit evaluation.

The top three panels of Figure 7 show the regional distributions of the global population as a function of hybrid $PM_{2.5}$ concentrations for 1998, 2008, and 2018, following the method of Apte et al.[83] The bottom panel shows the regional distributions of the global population as a function of the 1998−2018 trends from Figure 4. Only statistically significant (p-value <0.05) trends were included to focus on locations with meaningful trends; therefore, the populations in the bottom plot reflect those exposed to statistically significant trends, not the total populations.

For all three years (top panels), the majority of the global population (89% in 1998, 86% in 2008, 83% in 2018) lived in regions with $PM_{2.5}$ concentrations above the WHO air quality guideline of 10 $\mu g/m^3$. Over 1998−2018, 27% of the global population experienced statistically significant trends (p-value <0.5) (bottom panel). Statistically significant negative trends were experienced by 23% of the total North American and 23% of the total European populations, while 11% and 14% of the total populations respectively experienced statistically significant positive trends. The population of India exposed to $PM_{2.5}$ concentrations of 50−150 $\mu g/m^3$ increased from 46% in 1998 to 69% in 2018 (top panels), with 40% of the total population experiencing statistically significant positive trends (1 to 4 $\mu g/m^3/yr$) and 0% experiencing statistically significant negative trends (bottom panel). The fraction of the population in China exposed to $PM_{2.5}$ concentrations of 50−100 $\mu g/m^3$ increased in 2008 (56%) compared to 1998 (40%); however, the fraction significantly decreased in 2018 (18%) as more of the population shifted toward ∼50 $\mu g/m^3$. Over 1998−2018, 8% of the total population in China experienced statistically significant negative trends, while 13% experienced statistically significant positive trends. Globally, 8% of the total population experienced statistically significant negative trends, while 18% experienced statistically significant positive trends.

In summary, advances in satellite AOD, simulation, and ground monitor data enabled improved global $PM_{2.5}$ estimates and trends over the years 1998−2018, revealing large shifts in the global distribution of $PM_{2.5}$. The advances in satellite AOD data benefited from finer resolution (MISR), increased global availability (MAIAC), and updated radiometric calibration that improved the stability of all MODIS products over time. The advances in the GEOS-Chem simulation include consistent long-term meteorology (MERRA-2), developments to dust and SOA chemistry schemes, consistent biomass burning emissions for the entire time period, and updated anthropogenic emission inventories providing improved time-varying information for more recent years, especially over China and India. The geophysical $PM_{2.5}$ estimates exhibited significant agreement with ground monitors (R^2 = 0.81), providing confidence in the utility of the geophysical estimates in regions with low monitor density. Statistical fusion explained an 11% of the variance in the $PM_{2.5}$ estimates, yielding an overall agreement of R^2 = 0.92 with cross-validated ground monitor sites. The resultant $PM_{2.5}$ estimates exhibited greater consistency with ground-based measurements than achieved by earlier global estimates. Differences with prior estimates of 20 $\mu g/m^3$ were found over large areas. Global population-weighted $PM_{2.5}$ estimates found here are 8.8 $\mu g/m^3$ lower than

https://dx.doi.org/10.1021/acs.est.0c01764
Environ. Sci. Technol. 2020, 54, 7879−7890

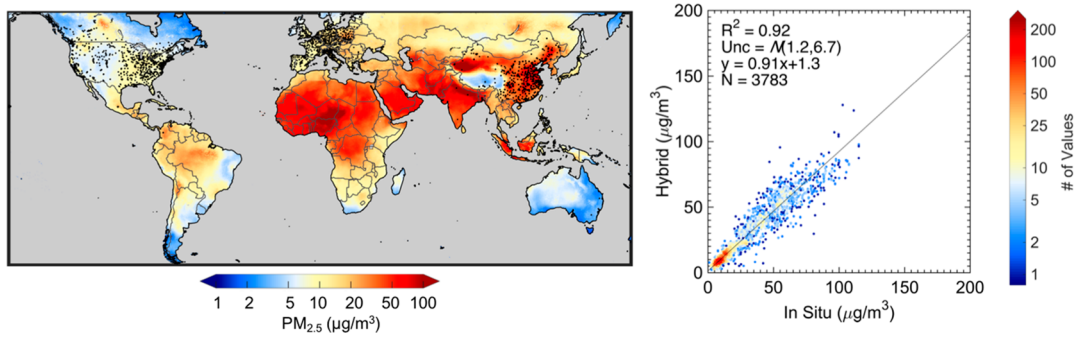

Figure 6. Left: Hybrid $PM_{2.5}$ for 2015. Black dots represent monitor locations. Gray denotes water. Right: Annual mean hybrid $PM_{2.5}$ versus coincident annual mean in situ values for 2015. Included on the plots are the coefficient of variation (R^2), the normal distribution of uncertainty (N(bias, variance)), the line of best fit (y), and the number of comparison points (N). The color-scale indicates the number density of observations at each point.

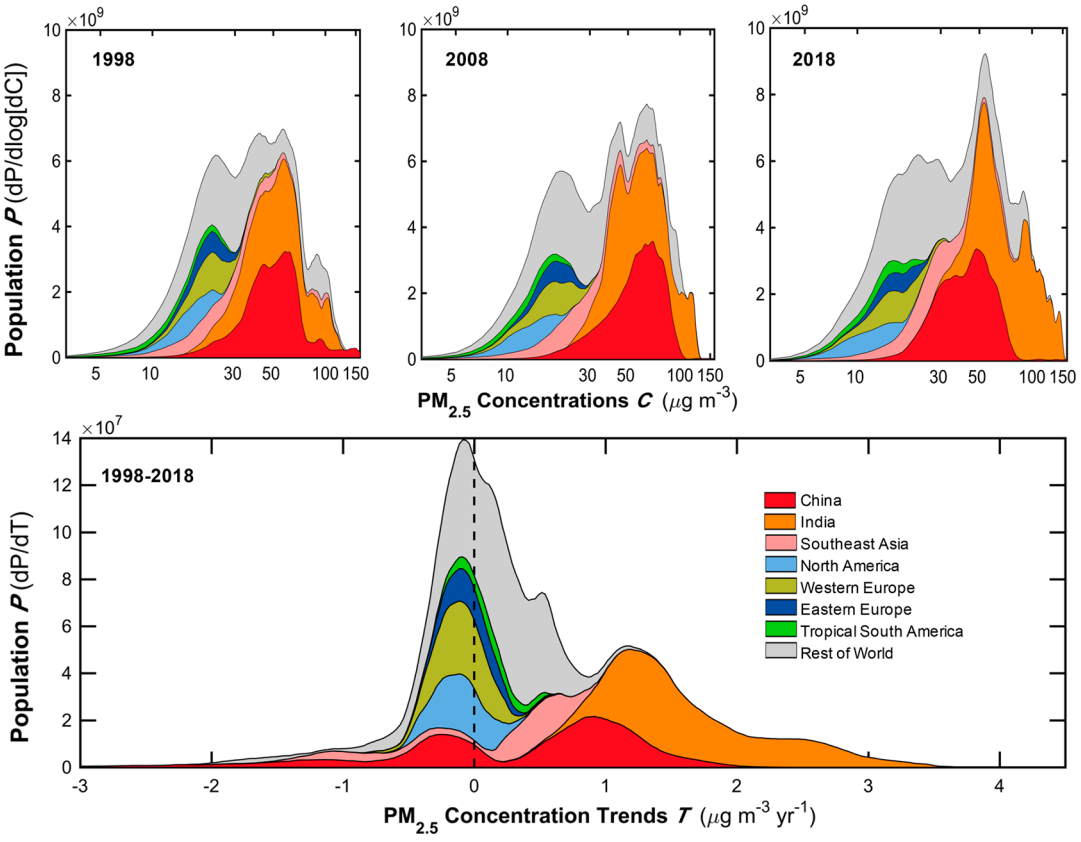

Figure 7. Top: Regional distribution of population as a function of $PM_{2.5}$ concentrations for 1998 (left), 2008 (middle), and 2018 (right). Plotted data reflect local smoothing of bin-width normalized distributions computed over 400 logarithmically spaced bins (range 0.1−400 $\mu g\ m^{-3}$) following the work of Apte et al.:[83] equal-sized plotted areas reflect equal populations. Population estimates are from the Gridded Population of the World (GPW v4) database.[87] The 2018 population estimate was obtained by linearly interpolating between 2015 and 2020. Bottom: Regional distribution of population (for 2018) as a function of 1998−2018 $PM_{2.5}$ trends with statistical significance (p-value <0.05).

recent estimates for the Global Burden of Disease. The remarkable trends found here for India and China illustrate the need for ongoing assessment of ambient $PM_{2.5}$ concentrations.

The temporal resolution of these globally fused $PM_{2.5}$ estimates focused on annual mean values to inform global health assessments, and to align with the time scale at which ground-based observations are readily available at a global scale. Regional monthly estimates have been developed for North America, Europe, and China (van Donkelaar et al.[84]), where ground measurements are available at higher frequency to evaluate and improve the estimates. Ongoing efforts to improve accessibility to higher frequency measurements, such as OpenAQ (https://openaq.org), may allow increased global temporal resolution in the future. Additional ground-based monitoring of co-located AOD and $PM_{2.5}$ (e.g., https://openaq.org) would offer valuable information to evaluate and improve simulation of the AOD-to-$PM_{2.5}$ relationship and in turn satellite-derived estimates of $PM_{2.5}$.[85,86]

The global $PM_{2.5}$ estimates described in this work are publicly available as version V4.GL.03 via the Atmospheric Composition Analysis Group Web site at Dalhousie University (http://fizz.phys.dal.ca/~atmos/martin/?page_id=140http://

https://dx.doi.org/10.1021/acs.est.0c01764
Environ. Sci. Technol. 2020, 54, 7879−7890

fizz.phys.dal.ca/~atmos/martin/?page_id=140) and Washington University (http://sites.wustl.edu/acag), or by contacting the authors.

■ ASSOCIATED CONTENT

Supporting Information

The Supporting Information is available free of charge at https://pubs.acs.org/doi/10.1021/acs.est.0c01764.

Detailed description of satellite AOD sources, GEOS-Chem simulation, and algorithm for calculating $PM_{2.5}$ estimates (PDF)

■ AUTHOR INFORMATION

Corresponding Author

Melanie S. Hammer − *Department of Energy, Environmental & Chemical Engineering, Washington University in St. Louis, St. Louis, Missouri 63130, United States; Department of Physics and Atmospheric Science, Dalhousie University, Halifax, N.S. B3H3J5, Canada;* orcid.org/0000-0001-8443-7979; Email: melanie.hammer@wustl.edu

Authors

Aaron van Donkelaar − *Department of Energy, Environmental & Chemical Engineering, Washington University in St. Louis, St. Louis, Missouri 63130, United States; Department of Physics and Atmospheric Science, Dalhousie University, Halifax, N.S. B3H3J5, Canada;* orcid.org/0000-0002-2998-8521

Chi Li − *Department of Physics and Atmospheric Science, Dalhousie University, Halifax, N.S. B3H3J5, Canada; Department of Chemistry, University of California, Berkeley, Berkeley, California 94720, United States;* orcid.org/0000-0002-8992-7026

Alexei Lyapustin − *Earth Sciences Division, NASA Goddard Space Flight Center, Greenbelt, Maryland 20771, United States; Goddard Earth Sciences Technology and Research, Universities Space Research Association, Greenbelt, Maryland 20771, United States*

Andrew M. Sayer − *Earth Sciences Division, NASA Goddard Space Flight Center, Greenbelt, Maryland 20771, United States; Goddard Earth Sciences Technology and Research, Universities Space Research Association, Greenbelt, Maryland 20771, United States*

N. Christina Hsu − *Earth Sciences Division, NASA Goddard Space Flight Center, Greenbelt, Maryland 20771, United States*

Robert C. Levy − *Earth Sciences Division, NASA Goddard Space Flight Center, Greenbelt, Maryland 20771, United States*

Michael J. Garay − *Jet Propulsion Laboratory, California Institute of Technology, Pasadena, California 91125-0002, United States*

Olga V. Kalashnikova − *Jet Propulsion Laboratory, California Institute of Technology, Pasadena, California 91125-0002, United States*

Ralph A. Kahn − *Earth Sciences Division, NASA Goddard Space Flight Center, Greenbelt, Maryland 20771, United States*

Michael Brauer − *School of Population and Public Health, The University of British Columbia, Vancouver, British Columbia V6T1Z3, Canada; Institute for Health Metrics and Evaluation, University of Washington, Seattle 98121, United States;* orcid.org/0000-0002-9103-9343

Joshua S. Apte − *Department of Civil, Architectural and Environmental Engineering, University of Texas at Austin, Austin, Texas 78712, United States;* orcid.org/0000-0002-2796-3478

Daven K. Henze − *Department of Mechanical Engineering, University of Colorado Boulder, Boulder, Colorado 80309, United States*

Li Zhang − *CIRES, University of Colorado, Boulder, Colorado 80309, United States; Global Systems Division, Earth System Research Laboratory, NOAA, Boulder, Colorado 80309, United States*

Qiang Zhang − *Ministry of Education Key Laboratory for Earth System Modeling, Department of Earth System Science, Tsinghua University, Beijing 100084, China; Collaborative Innovation Center for Regional Environmental Quality, Beijing 100084, China*

Bonne Ford − *Department of Atmospheric Science, Colorado State University, Fort Collins 80523-1019, United States*

Jeffrey R. Pierce − *Department of Atmospheric Science, Colorado State University, Fort Collins 80523-1019, United States;* orcid.org/0000-0002-4241-838X

Randall V. Martin − *Department of Energy, Environmental & Chemical Engineering, Washington University in St. Louis, St. Louis, Missouri 63130, United States; Department of Physics and Atmospheric Science, Dalhousie University, Halifax, N.S. B3H3J5, Canada; Harvard-Smithsonian Center for Astrophysics, Cambridge, Massachusetts 02138, United States*

Complete contact information is available at: https://pubs.acs.org/10.1021/acs.est.0c01764

Notes

The authors declare no competing financial interest.

■ ACKNOWLEDGMENTS

This work was supported by the Natural Sciences and Engineering Research Council (NSERC), the Energy Policy Institute at the University of Chicago, and the Health Effects Institute. M.H. was partially supported by the Killam Trusts. GEOS-Chem input files were obtained from the GEOS-Chem Data Portal enabled by Compute Canada.

■ REFERENCES

(1) GBD 2016 risk factors: Gakidou, E.; Afshin, A.; Abajobir, A. A.; Abate, K. H.; Abbafati, C.; Abbas, K. M.; Abd-Allah, F.; Abdulle, A. M.; Abera, S. F.; Aboyans, V.; et al. Global, Regional, and National Comparative Risk Assessment of 84 Behavioural, Environmental and Occupational, and Metabolic Risks or Clusters of Risks, 1990−2016: A Systematic Analysis for the Global Burden of Disease Study 2016. *Lancet* **2017**, *390* (10100), 1345−1422.

(2) Health Effects Institute. State of Global Air 2019; Health Effects Institute, 2019.

(3) *The Economic Consequences of Outdoor Air Pollution*; OECD: Paris, 2016; DOI: DOI: 10.1787/9789264257474-en.

(4) Greenstone, M.; Fan, C. Q. Introducing the Air Quality Life Index Twelve Facts about Particulate Air Pollution, Human Health, and Global Policy Index; University of Chicago, 2018.

(5) Martin, R. V.; Brauer, M.; van Donkelaar, A.; Shaddick, G.; Narain, U.; Dey, S. No One Knows Which City Has the Highest Concentration of Fine Particulate Matter. *Atmos. Environ. X* **2019**, *3*, 100040.

(6) West, J. J.; Cohen, A.; Dentener, F.; Brunekreef, B.; Zhu, T.; Armstrong, B.; Bell, M. L.; Brauer, M.; Carmichael, G.; Costa, D. L.; Dockery, D. W.; Kleeman, M.; Krzyzanowski, M.; Künzli, N.; Liousse, C.; Lung, S.-C. C.; Martin, R. V.; Pöschl, U.; Pope, C. A.; Roberts, J. M.; Russell, A. G.; Wiedinmyer, C. What We Breathe Impacts Our

Health: Improving Understanding of the Link between Air Pollution and Health. *Environ. Sci. Technol.* **2016**, *50* (10), 4895−4904.
(7) Gupta, P.; Levy, R. C.; Mattoo, S.; Remer, L. A.; Munchak, L. A. A Surface Reflectance Scheme for Retrieving Aerosol Optical Depth over Urban Surfaces in MODIS Dark Target Retrieval Algorithm. *Atmos. Meas. Tech.* **2016**, *9* (7), 3293−3308.
(8) Sayer, A. M.; Hsu, N. C.; Lee, J.; Kim, W. V.; Dutcher, S. T. Validation, Stability, and Consistency of MODIS Collection 6.1 and VIIRS Version 1 Deep Blue Aerosol Data Over Land. *J. Geophys. Res.: Atmos.* **2019**, *124* (8), 4658−4688.
(9) Hsu, N. C.; Lee, J.; Sayer, A. M.; Kim, W.; Bettenhausen, C.; Tsay, S.-C. VIIRS Deep Blue Aerosol Products Over Land: Extending the EOS Long-Term Aerosol Data Records. *J. Geophys. Res.: Atmos.* **2019**, *124* (7), 4026−4053.
(10) Lyapustin, A.; Wang, Y.; Korkin, S.; Huang, D. MODIS Collection 6 MAIAC Algorithm. *Atmos. Meas. Tech.* **2018**, *11* (10), 5741−5765.
(11) Garay, M. J.; Kalashnikova, O. V.; Bull, M. A. Development and Assessment of a Higher-Spatial-Resolution (4.4km) MISR Aerosol Optical Depth Product Using AERONET-DRAGON Data. *Atmos. Chem. Phys.* **2017**, *17* (8), 5095−5106.
(12) Franklin, M.; Kalashnikova, O. V.; Garay, M. J. Size-Resolved Particulate Matter Concentrations Derived from 4.4 Km-Resolution Size-Fractionated Multi-Angle Imaging SpectroRadiometer (MISR) Aerosol Optical Depth over Southern California. *Remote Sens. Environ.* **2017**, *196*, 312−323.
(13) Gelaro, R.; McCarty, W.; Suarez, M. J.; Todling, R.; Molod, A.; Takacs, L.; Randles, C. A.; Darmenov, A.; Bosilovich, M. G.; Reichle, R.; Wargan, K.; Coy, L.; Cullather, R.; Draper, C.; Akella, S.; Buchard, V.; Conaty, A.; da Silva, A. M.; Gu, W.; Kim, G.-K.; Koster, R.; Lucchesi, R.; Merkova, D.; Nielsen, J. E.; Partyka, G.; Pawson, S.; Putman, W.; Rienecker, M.; Schubert, S. D.; Sienkiewicz, M.; Zhao, B. The Modern-Era Retrospective Analysis for Research and Applications, Version 2 (MERRA-2). *J. Clim.* **2017**, *30* (14), 5419−5454.
(14) Marais, E. A.; Jacob, D. J.; Jimenez, J. L.; Campuzano-Jost, P.; Day, D. A.; Hu, W.; Krechmer, J.; Zhu, L.; Kim, P. S.; Miller, C. C.; Fisher, J. A.; Travis, K.; Yu, K.; Hanisco, T. F.; Wolfe, G. M.; Arkinson, H. L.; Pye, H. O. T.; Froyd, K. D.; Liao, J.; McNeill, V. F. Aqueous-Phase Mechanism for Secondary Organic Aerosol Formation from Isoprene: Application to the Southeast United States and Co-Benefit of SO_2 Emission Controls. *Atmos. Chem. Phys.* **2016**, *16* (3), 1603−1618.
(15) Pye, H. O. T.; Chan, A. W. H.; Barkley, M. P.; Seinfeld, J. H. Global Modeling of Organic Aerosol: The Importance of Reactive Nitrogen (NO_X and NO_3). *Atmos. Chem. Phys.* **2010**, *10* (22), 11261−11276.
(16) Ginoux, P.; Prospero, J. M.; Gill, T. E.; Hsu, N. C.; Zhao, M. Global-Scale Attribution of Anthropogenic and Natural Dust Sources and Their Emission Rates Based on MODIS Deep Blue Aerosol Products. *Rev. Geophys.* **2012**, DOI: 10.1029/2012RG000388.
(17) Zhang, L.; Kok, J. F.; Henze, D. K.; Li, Q.; Zhao, C. Improving Simulations of Fine Dust Surface Concentrations over the Western United States by Optimizing the Particle Size Distribution. *Geophys. Res. Lett.* **2013**, *40* (12), 3270−3275.
(18) Philip, S.; Martin, R. V.; Snider, G.; Weagle, C. L.; van Donkelaar, A.; Brauer, M.; Henze, D. K.; Klimont, Z.; Venkataraman, C.; Guttikunda, S. K.; Zhang, Q. Anthropogenic Fugitive, Combustion and Industrial Dust Is a Significant, Underrepresented Fine Particulate Matter Source in Global Atmospheric Models. *Environ. Res. Lett.* **2017**, *12* (4), 044018.
(19) Giglio, L.; Randerson, J. T.; van der Werf, G. R. Analysis of Daily, Monthly, and Annual Burned Area Using the Fourth-Generation Global Fire Emissions Database (GFED4). *J. Geophys. Res.: Biogeosci.* **2013**, *118* (1), 317−328.
(20) Li, M.; Zhang, Q.; Kurokawa, J.; Woo, J.-H.; He, K.; Lu, Z.; Ohara, T.; Song, Y.; Streets, D. G.; Carmichael, G. R.; Cheng, Y.; Hong, C.; Huo, H.; Jiang, X.; Kang, S.; Liu, F.; Su, H.; Zheng, B. MIX: A Mosaic Asian Anthropogenic Emission Inventory under the International Collaboration Framework of the MICS-Asia and HTAP. *Atmos. Chem. Phys.* **2017**, *17* (2), 935−963.
(21) Travis, K. R.; Jacob, D. J.; Fisher, J. A.; Kim, P. S.; Marais, E. A.; Zhu, L.; Yu, K.; Miller, C. C.; Yantosca, R. M.; Sulprizio, M. P.; Thompson, A. M.; Wennberg, P. O.; Crounse, J. D.; St. Clair, J. M.; Cohen, R. C.; Laughner, J. L.; Dibb, J. E.; Hall, S. R.; Ullmann, K.; Wolfe, G. M.; Pollack, I. B.; Peischl, J.; Neuman, J. A.; Zhou, X. Why Do Models Overestimate Surface Ozone in the Southeast United States? *Atmos. Chem. Phys.* **2016**, *16* (21), 13561−13577.
(22) World Health Organization. *WHO Global Ambient Air Quality Database (Update 2018)*; WHO: Geneva, 2018.
(23) Kumar, N.; Chu, A.; Foster, A. An Empirical Relationship between PM2.5 and Aerosol Optical Depth in Delhi Metropolitan. *Atmos. Environ.* **2007**, *41* (21), 4492−4503.
(24) Liu, Y.; Sarnat, J. A.; Kilaru, V.; Jacob, D. J.; Koutrakis, P. Estimating Ground-Level PM2.5 in the Eastern United States Using Satellite Remote Sensing. *Environ. Sci. Technol.* **2005**, *39* (9), 3269−3278.
(25) de Hoogh, K.; Chen, J.; Gulliver, J.; Hoffmann, B.; Hertel, O.; Ketzel, M.; Bauwelinck, M.; van Donkelaar, A.; Hvidtfeldt, U. A.; Katsouyanni, K.; Klompmaker, J.; Martin, R. V.; Samoli, E.; Schwartz, P. E.; Stafoggia, M.; Bellander, T.; Strak, M.; Wolf, K.; Vienneau, D.; Brunekreef, B.; Hoek, G. Spatial PM2.5, NO2, O3 and BC Models for Western Europe − Evaluation of Spatiotemporal Stability. *Environ. Int.* **2018**, *120*, 81−92.
(26) Ma, Z.; Hu, X.; Huang, L.; Bi, J.; Liu, Y. Estimating Ground-Level PM $_{2.5}$ in China Using Satellite Remote Sensing. *Environ. Sci. Technol.* **2014**, *48* (13), 7436−7444.
(27) Song, W.; Jia, H.; Huang, J.; Zhang, Y. A Satellite-Based Geographically Weighted Regression Model for Regional PM2.5 Estimation over the Pearl River Delta Region in China. *Remote Sens. Environ.* **2014**, *154*, 1−7.
(28) van Donkelaar, A.; Martin, R. V.; Brauer, M.; Boys, B. L. Use of Satellite Observations for Long-Term Exposure Assessment of Global Concentrations of Fine Particulate Matter. *Environ. Health Perspect.* **2015**, *123* (2), 135−143.
(29) van Donkelaar, A.; Martin, R. V.; Brauer, M.; Hsu, N. C.; Kahn, R. A.; Levy, R. C.; Lyapustin, A.; Sayer, A. M.; Winker, D. M. Global Estimates of Fine Particulate Matter Using a Combined Geophysical-Statistical Method with Information from Satellites, Models, and Monitors. *Environ. Sci. Technol.* **2016**, *50* (7), 3762−3772.
(30) Shaddick, G.; Thomas, M. L.; Green, A.; Brauer, M.; van Donkelaar, A.; Burnett, R.; Chang, H. H.; Cohen, A.; van Dingenen, R.; Dora, C.; Gumy, S.; Liu, Y.; Martin, R.; Waller, L. A.; West, J.; Zidek, J. V.; Prüss-Ustün, A. Data Integration Model for Air Quality: A Hierarchical Approach to the Global Estimation of Exposures to Ambient Air Pollution. *J. R. Stat. Soc. Ser. C (Applied Stat.* **2018**, *67* (1), 231−253.
(31) Di, Q.; Koutrakis, P.; Schwartz, J. A Hybrid Prediction Model for PM2.5 Mass and Components Using a Chemical Transport Model and Land Use Regression. *Atmos. Environ.* **2016**, *131*, 390−399.
(32) Friberg, M. D.; Kahn, R. A.; Holmes, H. A.; Chang, H. H.; Sarnat, S. E.; Tolbert, P. E.; Russell, A. G.; Mulholland, J. A. Daily Ambient Air Pollution Metrics for Five Cities: Evaluation of Data-Fusion-Based Estimates and Uncertainties. *Atmos. Environ.* **2017**, *158*, 36−50.
(33) Kunzli, N. Assessment of Deaths Attributable to Air Pollution: Should We Use Risk Estimates Based on Time Series or on Cohort Studies? *Am. J. Epidemiol.* **2001**, *153* (11), 1050−1055.
(34) Brook, R. D.; Rajagopalan, S.; Pope, C. A.; Brook, J. R.; Bhatnagar, A.; Diez-Roux, A. V.; Holguin, F.; Hong, Y.; Luepker, R. V.; Mittleman, M. A.; Peters, A.; Siscovick, D.; Smith, S. C.; Whitsel, L.; Kaufman, J. D. American Heart Association Council on Epidemiology and Prevention, Council on the Kidney in Cardiovascular Disease, and Council on Nutrition, Physical Activity and Metabolism. Particulate Matter Air Pollution and Cardiovascular Disease. *Circulation* **2010**, *121* (21), 2331−2378.

https://dx.doi.org/10.1021/acs.est.0c01764
Environ. Sci. Technol. 2020, 54, 7879−7890

(35) Pope, C. A. Mortality Effects of Longer Term Exposures to Fine Particulate Air Pollution: Review of Recent Epidemiological Evidence. *Inhalation Toxicol.* **2007**, *19* (sup1), 33−38.
(36) Yitshak-Sade, M.; Bobb, J. F.; Schwartz, J. D.; Kloog, I.; Zanobetti, A. The Association between Short and Long-Term Exposure to PM2.5 and Temperature and Hospital Admissions in New England and the Synergistic Effect of the Short-Term Exposures. *Sci. Total Environ.* **2018**, *639*, 868−875.
(37) Liang, F.; Xiao, Q.; Gu, D.; Xu, M.; Tian, L.; Guo, Q.; Wu, Z.; Pan, X.; Liu, Y. Satellite-Based Short- and Long-Term Exposure to PM2.5 and Adult Mortality in Urban Beijing, China. *Environ. Pollut.* **2018**, *242*, 492−499.
(38) Sayer, A. M.; Munchak, L. A.; Hsu, N. C.; Levy, R. C.; Bettenhausen, C.; Jeong, M.-J. MODIS Collection 6 Aerosol Products: Comparison between Aqua's e-Deep Blue, Dark Target, and "Merged" Data Sets, and Usage Recommendations. *J. Geophys. Res. Atmos.* **2014**, *119* (24), 13965−13989.
(39) Levy, R. C.; Mattoo, S.; Munchak, L. A.; Remer, L. A.; Sayer, A. M.; Patadia, F.; Hsu, N. C. The Collection 6 MODIS Aerosol Products over Land and Ocean. *Atmos. Meas. Tech.* **2013**, *6* (11), 2989−3034.
(40) Sayer, A. M.; Hsu, N. C.; Bettenhausen, C.; Jeong, M.-J.; Holben, B. N.; Zhang, J. Global and Regional Evaluation of Over-Land Spectral Aerosol Optical Depth Retrievals from SeaWiFS. *Atmos. Meas. Tech.* **2012**, *5* (7), 1761−1778.
(41) Hsu, N. C.; Jeong, M.-J.; Bettenhausen, C.; Sayer, A. M.; Hansell, R.; Seftor, C. S.; Huang, J.; Tsay, S.-C. Enhanced Deep Blue Aerosol Retrieval Algorithm: The Second Generation. *J. Geophys. Res. Atmos.* **2013**, *118* (16), 9296−9315.
(42) Diner, D. J.; Beckert, J. C.; Reilly, T. H.; Bruegge, C. J.; Conel, J. E.; Kahn, R. A.; Martonchik, J. V.; Ackerman, T. P.; Davies, R.; Gerstl, S. A. W.; Gordon, H. R.; Muller, J.; Myneni, R. B.; Sellers, P. J.; Pinty, B.; Verstraete, M. M. Multi-Angle Imaging SpectroRadiometer (MISR) Instrument Description and Experiment Overview. *IEEE Trans. Geosci. Remote Sens.* **1998**, *36* (4), 1072−1087.
(43) Martonchik, J. V.; Kahn, R. A.; Diner, D. J. Retrieval of Aerosol Properties over Land Using MISR Observations. In *Satellite Aerosol Remote Sensing over Land*; Springer: Berlin, 2009; pp 267−293. DOI: DOI: 10.1007/978-3-540-69397-0_9.
(44) Garay, M. J.; Witek, M. L.; Kahn, R. A.; Seidel, F. C.; Limbacher, J. A.; Bull, M. A.; Diner, D. J.; Hansen, E. G.; Kalashnikova, O. V.; Lee, H.; Nastan, A. M.; Yu, Y. Introducing the 4.4km Spatial Resolution Multi-Angle Imaging SpectroRadiometer (MISR) Aerosol Product. *Atmos. Meas. Tech.* **2020**, *13* (2), 593−628.
(45) van Donkelaar, A.; Martin, R. V.; Brauer, M.; Kahn, R.; Levy, R.; Verduzco, C.; Villeneuve, P. J. Global Estimates of Ambient Fine Particulate Matter Concentrations from Satellite-Based Aerosol Optical Depth: Development and Application. *Environ. Health Perspect.* **2010**, *118* (6), 847−855.
(46) Van Donkelaar, A.; Martin, R. V.; Park, R. J. Estimating Ground-Level PM 2.5 Using Aerosol Optical Depth Determined from Satellite Remote Sensing. *J. Geophys. Res.* **2006**, *111*, 21201.
(47) Molod, A.; Takacs, L.; Suarez, M.; Bacmeister, J. Development of the GEOS-5 Atmospheric General Circulation Model: Evolution from MERRA to MERRA2. *Geosci. Model Dev.* **2015**, *8* (5), 1339−1356.
(48) Lu, Z.; Zhang, Q.; Streets, D. G. Sulfur Dioxide and Primary Carbonaceous Aerosol Emissions in China and India. *Atmos. Chem. Phys.* **2011**, *11*, 9839−9864.
(49) Holben, B. N.; Eck, T. F.; Slutsker, I.; Tanré, D.; Buis, J. P.; Setzer, A.; Vermote, E.; Reagan, J. A.; Kaufman, Y. J.; Nakajima, T.; Lavenu, F.; Jankowiak, I.; Smirnov, A. AERONET—A Federated Instrument Network and Data Archive for Aerosol Characterization. *Remote Sens. Environ.* **1998**, *66* (1), 1−16.
(50) Eck, T. F.; Holben, B. N.; Reid, J. S.; Dubovik, O.; Smirnov, A.; O'Neill, N. T.; Slutsker, I.; Kinne, S. Wavelength Dependence of the Optical Depth of Biomass Burning, Urban, and Desert Dust Aerosols. *J. Geophys. Res. Atmos.* **1999**, *104* (D24), 31333−31349.
(51) Giles, D. M.; Sinyuk, A.; Sorokin, M. G.; Schafer, J. S.; Smirnov, A.; Slutsker, I.; Eck, T. F.; Holben, B. N.; Lewis, J. R.; Campbell, J. R.; Welton, E. J.; Korkin, S. V.; Lyapustin, A. I. Advancements in the Aerosol Robotic Network (AERONET) Version 3 Database − Automated near-Real-Time Quality Control Algorithm with Improved Cloud Screening for Sun Photometer Aerosol Optical Depth (AOD) Measurements. *Atmos. Meas. Tech.* **2019**, *12* (1), 169−209.
(52) Li, Z.; Zhao, X.; Kahn, R.; Mishchenko, M.; Remer, L.; Lee, K.-H.; Wang, M.; Laszlo, I.; Nakajima, T.; Maring, H. Uncertainties in Satellite Remote Sensing of Aerosols and Impact on Monitoring Its Long-Term Trend: A Review and Perspective. *Ann. Geophys.* **2009**, *27* (7), 2755−2770.
(53) van Donkelaar, A.; Martin, R. V.; Spurr, R. J. D.; Drury, E.; Remer, L. A.; Levy, R. C.; Wang, J. Optimal Estimation for Global Ground-Level Fine Particulate Matter Concentrations. *J. Geophys. Res. Atmos.* **2013**, *118* (11), 5621−5636.
(54) Brunsdon, C.; Fotheringham, A. S.; Charlton, M. E. Geographically Weighted Regression: A Method for Exploring Spatial Nonstationarity. *Geogr. Anal.* **1996**, *28* (4), 281−298.
(55) Fotheringham, A. S.; Charlton, M. E.; Brunsdon, C. Geographically Weighted Regression: A Natural Evolution of the Expansion Method for Spatial Data Analysis. *Environ. Plan. A Econ. Sp.* **1998**, *30* (11), 1905−1927.
(56) Jin, X.; Fiore, A. M.; Curci, G.; Lyapustin, A.; Civerolo, K.; Ku, M.; van Donkelaar, A.; Martin, R. V. Assessing Uncertainties of a Geophysical Approach to Estimate Surface Fine Particulate Matter Distributions from Satellite-Observed Aerosol Optical Depth. *Atmos. Chem. Phys.* **2019**, *19* (1), 295−313.
(57) Wang, Y.; Chen, Y. Significant Climate Impact of Highly Hygroscopic Atmospheric Aerosols in Delhi, India. *Geophys. Res. Lett.* **2019**, *46* (10), 5535−5545.
(58) Wang, Y.; Wang, Y.; Wang, L.; Petäjä, T.; Zha, Q.; Gong, C.; Li, S.; Pan, Y.; Hu, B.; Xin, J.; Kulmala, M. Increased Inorganic Aerosol Fraction Contributes to Air Pollution and Haze in China. *Atmos. Chem. Phys.* **2019**, *19* (9), 5881−5888.
(59) He, Q.; Zhou, G.; Geng, F.; Gao, W.; Yu, W. Spatial Distribution of Aerosol Hygroscopicity and Its Effect on PM2.5 Retrieval in East China. *Atmos. Res.* **2016**, *170*, 161−167.
(60) Deng, X.; Tie, X.; Zhou, X.; Wu, D.; Zhong, L.; Tan, H.; Li, F.; Huang, X.; Bi, X.; Deng, T. Effects of Southeast Asia Biomass Burning on Aerosols and Ozone Concentrations over the Pearl River Delta (PRD) Region. *Atmos. Environ.* **2008**, *42* (36), 8493−8501.
(61) Zhang, M.; Wang, Y.; Ma, Y.; Wang, L.; Gong, W.; Liu, B. Spatial Distribution and Temporal Variation of Aerosol Optical Depth and Radiative Effect in South China and Its Adjacent Area. *Atmos. Environ.* **2018**, *188*, 120−128.
(62) Yao, L.; Yang, L.; Yuan, Q.; Yan, C.; Dong, C.; Meng, C.; Sui, X.; Yang, F.; Lu, Y.; Wang, W. Sources Apportionment of PM2.5 in a Background Site in the North China Plain. *Sci. Total Environ.* **2016**, *541*, 590−598.
(63) Timmermans, R.; Kranenburg, R.; Manders, A.; Hendriks, C.; Segers, A.; Dammers, E.; Zhang, Q.; Wang, L.; Liu, Z.; Zeng, L.; Denier van der Gon, H.; Schaap, M. Source Apportionment of PM2.5 across China Using LOTOS-EUROS. *Atmos. Environ.* **2017**, *164*, 370−386.
(64) Zong, Z.; Wang, X.; Tian, C.; Chen, Y.; Fu, S.; Qu, L.; Ji, L.; Li, J.; Zhang, G. PMF and PSCF Based Source Apportionment of PM2.5 at a Regional Background Site in North China. *Atmos. Res.* **2018**, *203*, 207−215.
(65) Lee, H.-H.; Iraqui, O.; Gu, Y.; Yim, S. H.-L.; Chulakadabba, A.; Tonks, A. Y.-M.; Yang, Z.; Wang, C. Impacts of Air Pollutants from Fire and Non-Fire Emissions on the Regional Air Quality in Southeast Asia. *Atmos. Chem. Phys.* **2018**, *18* (9), 6141−6156.
(66) Singh, N.; Murari, V.; Kumar, M.; Barman, S. C.; Banerjee, T. Fine Particulates over South Asia: Review and Meta-Analysis of PM2.5 Source Apportionment through Receptor Model. *Environ. Pollut.* **2017**, *223*, 121−136.
(67) Gherboudj, I.; Naseema Beegum, S.; Ghedira, H. Identifying Natural Dust Source Regions over the Middle-East and North-Africa:

https://dx.doi.org/10.1021/acs.est.0c01764
Environ. Sci. Technol. 2020, 54, 7879−7890

Estimation of Dust Emission Potential. *Earth-Sci. Rev.* **2017**, *165*, 342−355.
(68) Weagle, C. L.; Snider, G.; Li, C.; van Donkelaar, A.; Philip, S.; Bissonnette, P.; Burke, J.; Jackson, J.; Latimer, R.; Stone, E.; Abboud, I.; Akoshile, C.; Anh, N. X.; Brook, J. R.; Cohen, A.; Dong, J.; Gibson, M. D.; Griffith, D.; He, K. B.; Holben, B. N.; Kahn, R.; Keller, C. A.; Kim, J. S.; Lagrosas, N.; Lestari, P.; Khian, Y. L.; Liu, Y.; Marais, E. A.; Martins, J. V.; Misra, A.; Muliane, U.; Pratiwi, R.; Quel, E. J.; Salam, A.; Segev, L.; Tripathi, S. N.; Wang, C.; Zhang, Q.; Brauer, M.; Rudich, Y.; Martin, R. V. Global Sources of Fine Particulate Matter: Interpretation of PM $_{2.5}$ Chemical Composition Observed by SPARTAN Using a Global Chemical Transport Model. *Environ. Sci. Technol.* **2018**, DOI: 10.1021/acs.est.8b01658.
(69) Nayebare, S. R.; Aburizaiza, O. S.; Khwaja, H. A.; Siddique, A.; Hussain, M. M.; Zeb, J.; Khatib, F.; Carpenter, D. O.; Blake, D. R. Chemical Characterization and Source Apportionment of PM 2.5 in Rabigh, Saudi Arabia. *Aerosol Air Qual. Res.* **2016**, *16*, 3114−3129.
(70) Leibensperger, E. M.; Mickley, L. J.; Jacob, D. J.; Chen, W.-T.; Seinfeld, J. H.; Nenes, A.; Adams, P. J.; Streets, D. G.; Kumar, N.; Rind, D. Climatic Effects of 1950−2050 Changes in US Anthropogenic Aerosols − Part 2: Climate Response. *Atmos. Chem. Phys.* **2012**, *12* (7), 3349−3362.
(71) Klimont, Z.; Smith, S. J.; Cofala, J. The Last Decade of Global Anthropogenic Sulfur Dioxide: 2000−2011 Emissions. *Environ. Res. Lett.* **2013**, *8* (1), 14003−14006.
(72) Curier, L.; Kranenburg, R.; Timmermans, R.; Segers, A.; Eskes, H.; Schaap, M. *Synergistic Use of LOTOS-EUROS and NO2 Tropospheric Columns to Evaluate the NOX Emission Trends Over Europe* **2014**, 239−245.
(73) Simon, H.; Reff, A.; Wells, B.; Xing, J.; Frank, N. Ozone Trends Across the United States over a Period of Decreasing NOx and VOC Emissions. *Environ. Sci. Technol.* **2015**, *49* (1), 186−195.
(74) Xing, J.; Mathur, R.; Pleim, J.; Hogrefe, C.; Gan, C.-M.; Wong, D. C.; Wei, C.; Gilliam, R.; Pouliot, G. Observations and Modeling of Air Quality Trends over 1990−2010 across the Northern Hemisphere: China, the United States and Europe. *Atmos. Chem. Phys.* **2015**, *15* (5), 2723−2747.
(75) Li, C.; Martin, R. V.; van Donkelaar, A.; Boys, B. L.; Hammer, M. S.; Xu, J.-W.; Marais, E. A.; Reff, A.; Strum, M.; Ridley, D. A.; Crippa, M.; Brauer, M.; Zhang, Q. Trends in Chemical Composition of Global and Regional Population-Weighted Fine Particulate Matter Estimated for 25 Years. *Environ. Sci. Technol.* **2017**, *51*, 11185.
(76) Weatherhead, E. C.; Reinsel, G. C.; Tiao, G. C.; Meng, X.-L.; Choi, D.; Cheang, W.-K.; Keller, T.; DeLuisi, J.; Wuebbles, D. J.; Kerr, J. B.; Miller, A. J.; Oltmans, S. J.; Frederick, J. E. Factors Affecting the Detection of Trends: Statistical Considerations and Applications to Environmental Data. *J. Geophys. Res. Atmos.* **1998**, *103* (D14), 17149−17161.
(77) Weatherhead, E. C.; Stevermer, A. J.; Schwartz, B. E. Detecting Environmental Changes and Trends. *Phys. Chem. Earth, Parts A/B/C* **2002**, *27* (6−8), 399−403.
(78) Boys, B. L.; Martin, R. V.; van Donkelaar, A.; MacDonell, R. J.; Hsu, N. C.; Cooper, M. J.; Yantosca, R. M.; Lu, Z.; Streets, D. G.; Zhang, Q.; Wang, S. W. Fifteen-Year Global Time Series of Satellite-Derived Fine Particulate Matter. *Environ. Sci. Technol.* **2014**, *48* (19), 11109−11118.
(79) Klimont, Z.; Kupiainen, K.; Heyes, C.; Purohit, P.; Cofala, J.; Rafaj, P.; Borken-Kleefeld, J.; Schöpp, W. Global Anthropogenic Emissions of Particulate Matter Including Black Carbon. *Atmos. Chem. Phys.* **2017**, *17* (14), 8681−8723.
(80) Wang, S.; Zhang, Q.; Martin, R. V.; Philip, S.; Liu, F.; Li, M.; Jiang, X.; He, K. Satellite Measurements Oversee China's Sulfur Dioxide Emission Reductions from Coal-Fired Power Plants. *Environ. Res. Lett.* **2015**, *10* (11), 114015.
(81) Fioletov, V. E.; McLinden, C. A.; Krotkov, N.; Li, C.; Joiner, J.; Theys, N.; Carn, S.; Moran, M. D. A Global Catalogue of Large SO2 Sources and Emissions Derived from the Ozone Monitoring Instrument. *Atmos. Chem. Phys.* **2016**, *16* (18), 11497−11519.
(82) Zhai, S.; Jacob, D. J.; Wang, X.; Shen, L.; Li, K.; Zhang, Y.; Gui, K.; Zhao, T.; Liao, H. Fine Particulate Matter (PM2.5) Trends in China, 2013−2018: Separating Contributions from Anthropogenic Emissions and Meteorology. *Atmos. Chem. Phys.* **2019**, *19*, 11031−11041.
(83) Apte, J. S.; Marshall, J. D.; Cohen, A. J.; Brauer, M. Addressing Global Mortality from Ambient PM $_{2.5}$. *Environ. Sci. Technol.* **2015**, *49* (13), 8057−8066.
(84) van Donkelaar, A.; Martin, R. V.; Li, C.; Burnett, R. T. Regional Estimates of Chemical Composition of Fine Particulate Matter Using a Combined Geoscience-Statistical Method with Information from Satellites, Models, and Monitors. *Environ. Sci. Technol.* **2019**, *53* (5), 2595−2611.
(85) Snider, G.; Weagle, C. L.; Martin, R. V.; van Donkelaar, A.; Conrad, K.; Cunningham, D.; Gordon, C.; Zwicker, M.; Akoshile, C.; Artaxo, P.; Anh, N. X.; Brook, J.; Dong, J.; Garland, R. M.; Greenwald, R.; Griffith, D.; He, K.; Holben, B. N.; Kahn, R.; Koren, I.; Lagrosas, N.; Lestari, P.; Ma, Z.; Vanderlei Martins, J.; Quel, E. J.; Rudich, Y.; Salam, A.; Tripathi, S. N.; Yu, C.; Zhang, Q.; Zhang, Y.; Brauer, M.; Cohen, A.; Gibson, M. D.; Liu, Y. SPARTAN: A Global Network to Evaluate and Enhance Satellite-Based Estimates of Ground-Level Particulate Matter for Global Health Applications. *Atmos. Meas. Tech.* **2015**, *8* (1), 505−521.
(86) Snider, G.; Weagle, C. L.; Murdymootoo, K. K.; Ring, A.; Ritchie, Y.; Stone, E.; Walsh, A.; Akoshile, C.; Anh, N. X.; Balasubramanian, R.; Brook, J.; Qonitan, F. D.; Dong, J.; Griffith, D.; He, K.; Holben, B. N.; Kahn, R.; Lagrosas, N.; Lestari, P.; Ma, Z.; Misra, A.; Norford, L. K.; Quel, E. J.; Salam, A.; Schichtel, B.; Segev, L.; Tripathi, S.; Wang, C.; Yu, C.; Zhang, Q.; Zhang, Y.; Brauer, M.; Cohen, A.; Gibson, M. D.; Liu, Y.; Martins, J. V.; Rudich, Y.; Martin, R. V. Variation in Global Chemical Composition of PM $_{2.5}$: Emerging Results from SPARTAN. *Atmos. Chem. Phys.* **2016**, *16* (15), 9629−9653.
(87) CIESIN (Center for International Earth Science Information Network). *Gridded Population of the World Version 4*; NASA Socioeconomic Data and Applications Center (SEDAC): Palisades, NY, 2017; pp 1−21. DOI: DOI: 10.1128/AAC.03728-14.

https://dx.doi.org/10.1021/acs.est.0c01764
Environ. Sci. Technol. 2020, 54, 7879−7890